A New Current Probe with a Wide Bandwidth

Nicolas Karrer
Swiss Federal Institute of Technology
Electrical Engineering and Design Lab (EEK)
Gloriastrasse 35 / ETZ
CH-8092 Zürich
Switzerland
Tel: +41 1 632 7656
Fax: +41 1 632 1191
karrer@eek.ee.ethz.ch

Patrick Hofer-Noser
Atlantis Solar Systems
Lindenrain 4
CH-3012 Bern
Switzerland
Tel: +41 31 300 3280
Fax: +41 31 300 3290
hofer@atlantisenergy.ch

Daniel Henrard
LEM SA
Case Postale 785
CH-1212 Grand-Lancy 1
Switzerland
Tel: +41 22 706 1254
Fax: +41 22 794 9478
dhe@lem.com

Keywords

Measurement, Sensors, Power semiconductor devices, New devices, Rogowski coil, Hall sensor

Abstract

We present a new isolated current probe for power applications based on a Hall sensor as well as on a Rogowski coil. Employing these two sensors allows to eliminate the integrator circuit needed for the Rogowski signal. With this new probe DC currents as well as current transients with di/dt's of several kA/us can be measured.

1 Introduction

As a result of the ongoing power semiconductor development power devices, like IGBT's, allow to switch currents of some thousand amps in less than a microsecond. To keep the induced voltages as low as possible a low-inductance setup and short interconnections between the power elements are needed. A crucial problem is the current measurement in these low-inductance circuits needed for the detection of faults or for feedback control like the monitoring of paralleled IGBT's [1]. Therefore a current probe must be small in size and should not influence the power current signal. The probe should be isolated and capable of measuring DC currents of several hundred amps as well as transients in the order of several kA/us. A current probe was developed which satisfies these requirements. It consists of two well known current measuring principles: a Hall sensor for the low frequencies and a Rogowski coil for the high frequencies.

2 Theory

The main drawback when using a Hall sensor is its inability to measure high frequency current components. Drift and offset compensated Hall sensors such as spinning current sensors, have a low-pass characteristic with a cut-off frequency of some kHz. Hall sensors are used as stand-alone devices as well as in slotted cores [2] as part of a current compensated probe. These probes show a good performance at low frequencies but their main disadvantage appears when measuring higher frequencies where the compensating circuitry has to be as fast as the current to be measured.
Rogowski coil current probes are based on Faraday's induction law and can therefore not measure DC currents. According to Faraday's law, the output signal is proportional to the time derivative of the current to be measured. To obtain a signal which is proportional to the monitored current, the output signal of the coil must be integrated. This is a major disadvantage when constructing a Rogowski coil for current measurement [3,4,5,6].
Up to now the output signals of these two sensors have never been merged. This paper shows that using a special way to merge the output of the Hall sensor with the Rogowski coil, a current probe (Fig. 1) can be realized which combines the advantages of both sensors.

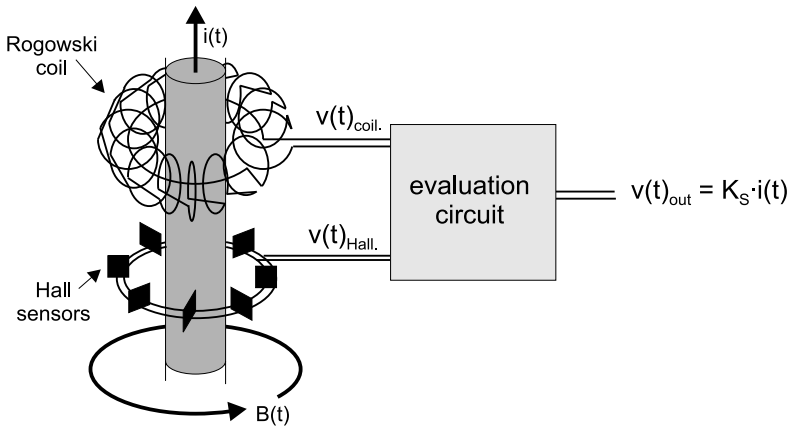

Fig. 1 : Current probe overview

2.1 Principle of operation

The output signal of a Hall sensor is proportional to the monitored current while the output signal of a Rogowski coil is proportional to the time derivative of the monitored current. Therefore we can model the Hall sensor as a low-pass and the coil as a differentiator. Fig. 2 shows a manner of merging both signals to get an output signal v(t) which is proportional to i(t) independent of the frequency components of i(t).

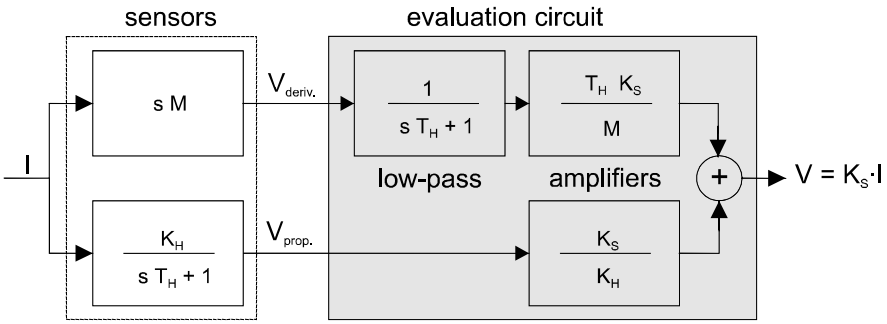

Fig. 2 : Ideal HOKA current measuring principle

M is the mutual induction between the primary current and the Rogowski coil. K_H and T_H are the model parameters of the Hall sensor. K_H is the Hall sensor sensitivity which depends on the distance from the copper bar as well as on the supply current. The corner frequency of the evaluation circuit's low-pass is matched to the corner frequency of the Hall sensor $\omega_H=1/T_H$. K_S/K_H is the sensitivity of the Hall signal path and T_H*K_S/M is the sensitivity of the coil signal path. Both signals are added to form the output signal v(t) of the probe. K_S is the sensitivity factor of the probe and it is considered to be K_S=1 V/1000 A in this paper. The transfer function (TF) of the probe (1) is a constant: $H(jw)=K_S$.

$$\frac{V(s)}{I(s)} = K_S\left[\frac{sT_H}{sT_H+1}\left(\frac{M}{M}\right)+\frac{1}{sT_H+1}\left(\frac{K_H}{K_H}\right)\right] = K_S\left[\frac{sT_H+1}{sT_H+1}\right] = K_S \qquad (1)$$

We called this principle of low-passing, scaling and adding HOKA principle, which shows a proportional TF. It can always be applied if the same source is measurable with sensors having a low-pass and a high-pass or derivative behavior. However, in the case of current measurement, it is not possible to construct a coil which demonstrates only a derivative behavior for all frequencies. A real coil has some resonance frequencies, but as shown later, they may be neglected in some specific cases.

2.2 Coil

Several coils of different topology have been realized as multi layer PCB's. These low cost coils showed an ideal inductive behavior till frequencies in the range of tens of MHz. Every winding is normal to the flux generated by the central current bar and is connected to the next winding on the outer circumference. Since the flux decreases with 1/r the winding geometry should be highly regular on the inner circumference. The return of the winding is placed in the inner layer as it is usual for Rogowski coils as shown in Fig. 3.

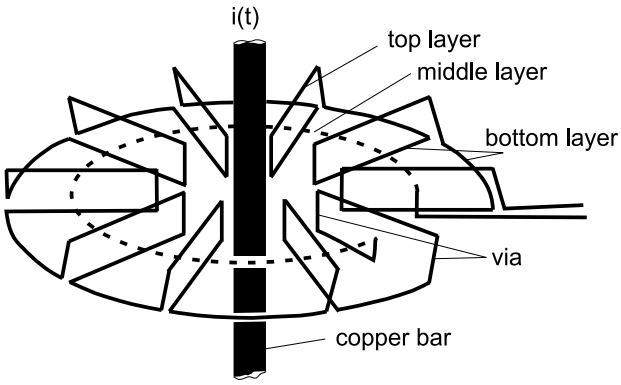

Fig. 3 : Coil topology

A model of the coil which approximates the coil's impedance till its first resonance frequency is given by (2). As shown in Fig. 4 the measurement (solid line) and simulation (dashed line) match very well.

$$Z(s) = \frac{s\,Lc + Rc}{s^2\,Cc\,Lc + s\,Cc\,Rc + 1} \quad (2)$$

Lc represents the self-inductance, Cc the interwinding capacitance and Rc the coil's wire resistance. For the simulation the following coil parameters have been used: Lc=1.55 uH, Cc=12.45 pF, Rc=3.4 Ohm.

The equation linking the primary current i(t) with the coil's output voltage $v_{emf}(t)$ can be approximated by (3) where Rd represents the load resistance of the following circuit, which should be in the range of some tens of kOhm. A low value of Rd reduces the resonant peak of the coil but at the same time the output signal differs from that of an ideal derivative signal [9]. M is the mutual inductance and its value is about M=12.2 nH for the described coil.

$$\frac{V_{emf}(s)}{I(s)} = \frac{s\,M}{s^2\,Lc\,Cc + s\left(\frac{Lc}{Rd} + Rc\,Cc\right) + \left(\frac{Rc}{Rd} + 1\right)} \quad (3)$$

The electrical model of the coil is given by the series connection of Lc, Rc and a voltage source. This branch is in parallel with Cc and Rd [9]. The voltage source is given by $v_{emf}(t)=M*di(t)/dt$.

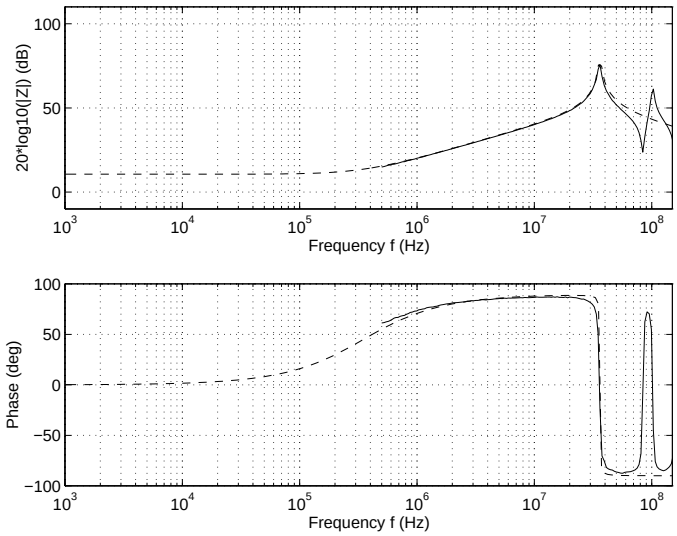

Fig. 4 : Impedance of coil Z(jw)

2.3 Hall sensor

Hall sensors can be approximated by a low-pass with a sensitivity of K_H and a corner frequency of $1/T_H$ (4). The corner frequency of the sensor depends on the semiconductor material and on the device type: a Hall sensor can have corner frequencies of some hundred kHz or higher while spinning current Hall sensors and sensors with an amplification stage show better temperature and linearity behavior but have a corner frequency of some kHz. For our setup a KSY 44 Hall sensor was used with a cutoff frequency of 1 MHz as advised by the manufacturer.

$$\frac{V_{Hall}(s)}{I(s)} = \frac{K_H}{sT_H + 1} \qquad (4)$$

When using a Hall sensor in a current compensated circuit [2] the effect of stray magnetic fields on the measurement is low because of the magnetic core except when the stray field is strong enough to saturate the core locally. The monitored current can also saturate the core or alter its residual magnetism by a surge current. Since a probe is wanted which is capable to measure up to high frequencies and which will not be damaged by surge currents, the Hall sensor is placed close to the current bar (Fig. 1) and no core material is used. The drawback of not concentrating the magnetic field through a core is that the sensor is prone to measure stray magnetic fields, especially the ones from the return bar. If the geometry of the magnetic field distribution is known, one or few Hall sensors can be used for an accurate measurement. When the field distribution is unknown, more Hall sensors are needed. The exact number of sensors to be placed around the current bar can be computed by applying Biot-Savart's law.

2.4 Simulation

The TF of the primary current i(t) to the output voltage $v_{emf}(t)$ of the coil can be approximated by (3) with the specified values of the components. The TF of the Hall sensor is given by (4) with T_H=1/(2*pi*1 MHz). The value of K_H and M are of no interest in the simulation since they are canceled out in (5). K_H, M and K_S are of interest when developing the evaluation circuit. They define the amplification value of the active low-pass. When several Hall sensors are used to increase the measurement accuracy and each sensor has a slightly different cutoff frequency, the block diagram of Fig. 2 must be changed to the one of Fig. 5.

Comparing Fig. 2 with Fig. 5 the following changes can be noted:

- The low-pass of the evaluation circuit has been moved past the addition block. This is a significant improvement when designing the evaluation circuit but the Hall sensor signal is now also fed through this low-pass.

- The corner frequency of the evaluation circuit's low-pass was changed to $\omega_V < \omega_H$. ω_V should be about 2 or more decades lower than the one of the Hall sensor so that its influence on the Hall signal can be neglected. The sensitivity of this low-pass is, with $T_V=1/(2*\pi*1\text{ kHz})$ and the above given values, $T_V*K_S/M=13$ representing a realizable amplification.
- The ideal coil has been replaced by a more realistic model where $T_2=\text{sqrt}(Lc*Cc)$, $T_1=Cc*Rc+Lc/Rd$ and $T_0=Rc/Rd+1$.

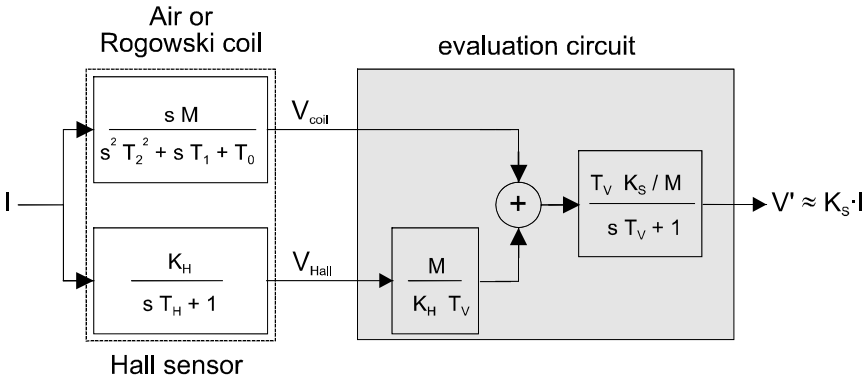

Fig. 5 : Practical realization

In this case the HOKA principle is not ideal anymore but the TF of the probe will be K_S till at least one decade before the resonance frequency of the coil. As long as neither the coil's TF nor the Hall sensor's TF differ from a constant value (in this case below 20 MHz) the TF of the current probe is constant.

$$\frac{V'(s)}{I(s)} = K_s\left[\frac{sT_V}{sT_V+1}\left(\frac{1}{s^2T_2^2+sT_1+T_0}\right)+\frac{1}{sT_V+1}\left(\frac{1}{sT_H+1}\right)\right] \quad (5)$$

Simulations of the expected TF (5) show this behavior in Fig. 6. The dashdotted line represents the low-pass and the dotted line with its peak at about 36 MHz is the TF of the coil. The dashed line shows the TF of the Hall sensor and the solid line represents the TF of the current probe based on (5).

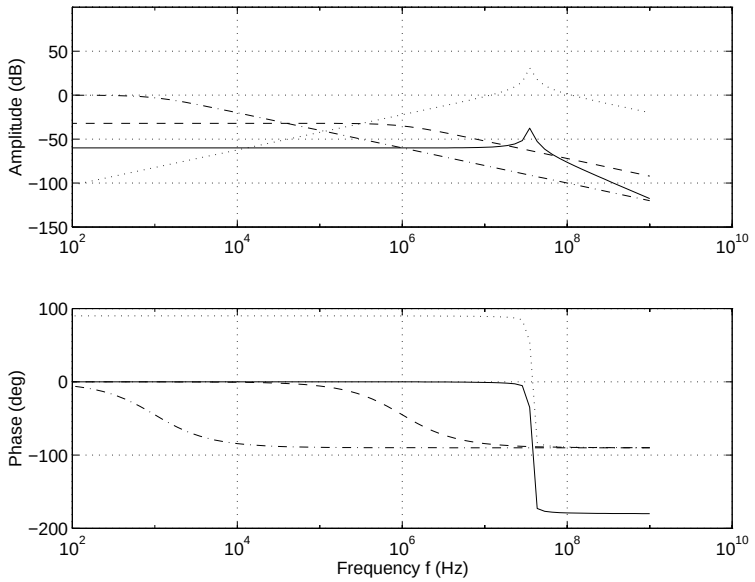

Fig. 6 : Bode plot of the probe's transfer function

2.5 Measurement error

The real Rogowski coil shows a second order system behavior. The TF of the probe will not be constant over the whole frequency domain as it is in the ideal case (1). In the following the influence

of the resonance frequency of the coil will be analyzed enabling us to predict the theoretical accuracy class of the probe based on a trapezoidal input signal. This signal was chosen since it is a very common current signal in power electronic applications. The accuracy class definition is given by (6) where $I_{FS\ probe}$ is the full-scale (FS) value, i_{output} is the value delivered by the probe and $i_{true\ value}$ is the value obtained by a perfect instrument.

$$i_{output} = i_{true\ value} \pm I_{FS\ probe}\left(\frac{\text{Class\_Index}}{100}\right) \qquad (6)$$

The class index is a number representing the accuracy class of an instrument. The definition (6) always refers to the maximal measurable value, the full scale value. Based on (6) we can therefore define a time dependent class index as follows:

$$\text{Class\_Index(t)} = \frac{\left|i(t) - i_{output}(t)\right|}{I_{FS\ probe}} 100 \qquad (7)$$

The class index of the probe is the maximum of (7) over one period of the current signal Fig. 7. For frequencies above the cutoff frequency ω_V of the low-pass, the TF of the probe can be approximated by (8). This can be seen when analyzing the Bode plot for higher frequencies: the –20 dB/dec asymptote of the low-pass is compensated by the +20 dB/dec asymptote of the coils derivative behavior. The Hall sensor contribution to the final signal can be neglected for high frequencies.

$$H(s) = \frac{K_s}{s^2 T_2^2 + s T_1 + T_0} \qquad (8)$$

We can further assume that the coil's undamped natural frequency is higher than the cutoff frequency of the low-pass. This was always the case for all constructed PCB coils. Since we want to use the coil as a derivative element, and not as a current transformer, the load resistor Rd should be chosen to be of some kOhm. Since Rc represents the coils wire resistance, which is in the order of some Ohms, the term T_0 is in the following assumed to be T_0=1.

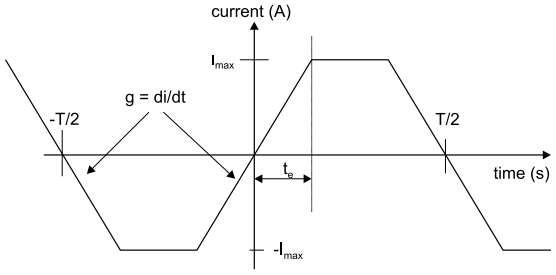

Fig. 7 : Trapezoidal waveform

Some more terms are introduced for convenience like the damping ratio d, the undamped natural frequency ω_n and the damped natural frequency ω_d of the coil, the time constant T_a as well as the term α and t_e (9).

$$d = \frac{1}{2}\frac{T_1}{T_2} \qquad \omega_n = \frac{1}{T_2} \qquad \alpha = \sqrt{1-d^2} \qquad \omega_d = \omega_n \alpha \qquad T_a = \frac{1}{d\,\omega_n} \qquad t_e = \frac{I_{\max}}{g} \qquad (9)$$

By using the Laplace transforms the response of the system (8) to the ramp r(t)=g*t, with g=di/dt being the slope of the ramp, was computed (10).

$$y(t) = g\,K_s\left[t - \frac{2d}{\omega_n} + \frac{1}{\omega_n \alpha} e^{\left(-\frac{t}{T_a}\right)} \sin(\omega_d t + \varphi)\right] \qquad (10)$$

$$\varphi = \arctan\left(\frac{2d\alpha}{2d^2 - 1}\right)$$

The probe's output signal will follow the ramp after a delay of $2*d/\omega_n$. To keep this delay as small as possible the damping ratio should be small while the undamped natural frequency should be high.

With d=0.1 and ω_n=2*π*36 MHz the delay is below one nanosecond. To reduce the influence of the third term as much as possible, the amplitude of the sine should be made small. This can be accomplished by a high ω_n and a small d as well as by reducing the time constant T_a by a high value of ω_n and d. This short analysis demonstrates that a coil with a high ω_n is always a good choice while d should be kept small. In any case d has to be smaller than 1. Knowing the ramp response of the probe, the absolute measurement error is defined by (11).

$$err(t) = \left| g\,t - \frac{1}{K_s}\,y(t) \right| \quad (11)$$

Note that the output signal of the probe must be back scaled by the factor 1/Ks. From (8) we can now compute the class index as a function of time (12).

$$\text{Class\_Index(t)} = \frac{err(t)}{I_{\text{FS probe}}} 100 \quad (12)$$

To keep the calculations simple, instead of computing the maximum over one trapezoidal waveform, only the error of a ramp signal has been considered, thus the transition of the signal from the steady state to the slope g. The worst case value for a ramp is given by (13).

$$\text{Class\_Index} = 100 \frac{g}{\omega_n\, I_{\text{FS probe}}} (0.66 d^3 - 0.18 d^2 + 0.53 d + 1) \quad (13)$$

The worst case for a trapezoidal waveform can be assumed to be smaller than twice the value of (13). Assuming a constant g=di/dt, the probe performs better with high than with low current, independent of the undamped natural frequency of the coil. For low current peaks with the same di/dt the coil must have a high ω_n. Fortunately this is not a major problem: we have built PCB coils of various resonance frequencies ranging from few MHz up to 180 MHz. The influence of the damping ratio d on the class varies from 1 (d=0) to 2 (d=1). For the coil we used in this paper, the undamped natural frequency is f_n = 36 MHz. Time domain simulations of the probe's behavior with a bounded ramp input signal or a trapezoidal input signal with di/dt=5 kA/us, f=20 kHz and a maximal amplitude of I_{max}=$I_{FS\ probe}$=3000 A and I_{max}=$I_{FS\ probe}$ =500 A show the effectiveness of (13).
The next four figures show time domain simulations of the TF (5). The left sub figures refer to a ramp input topping at I_{max} while the right sub figures refer to the above mentioned trapezoidal signal.
The top row displays the scaled input signal (solid line) and the probe's output signal (dashed). The bottom row is the representation of the class index. The computed class index for Fig. 9 with d=0.0083 is 0.74

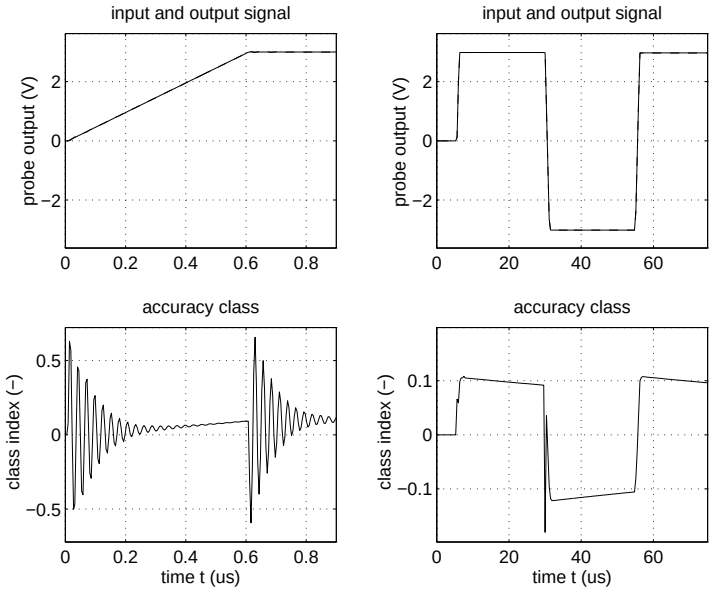

Fig. 8 : Time domain simulation, I_{max} = 3000 A, Rd = 50 kOhm

The computed class index for Fig. 9 with d=0.0083 is 4.41. This example shows the limitation of (13) which computes only the maximum class index of a not topped ramp. As mentioned before, the worst case for a trapezoidal waveform is twice the value, therefore the worst case class index is 8.8.

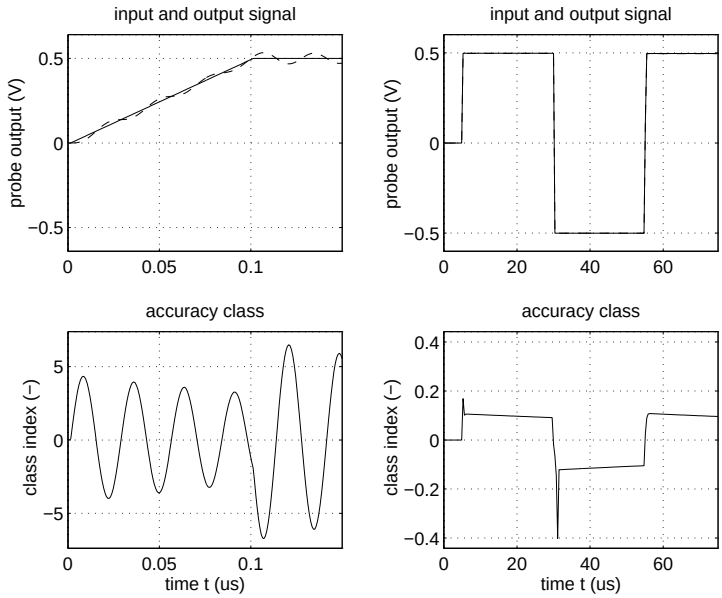

Fig. 9 : Time domain simulation, I_{max} = 500 A, Rd = 50 kOhm

The computed class index for Fig. 10 with d=0.88 is 1.29. This value is meaningless since the value of the damping resistor is chosen too low with Rd=200 Ohm. With a proper value for Rd the simulations of Fig. 8 are obtained. The value of the damping resistor should be high in order to obtain a derivative behavior for the coil [9].

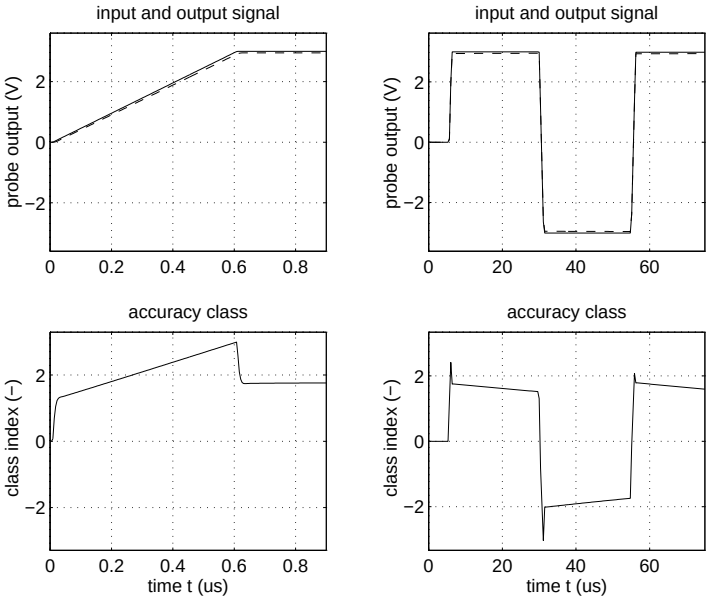

Fig. 10 : Time domain simulation, I_{max} = 3000 A, Rd = 200 Ohm

The computed class index for Fig. 11 with d=0.0083 is 0.88. Here the di/dt ratio was changed to g=di/dt=1kA/us.

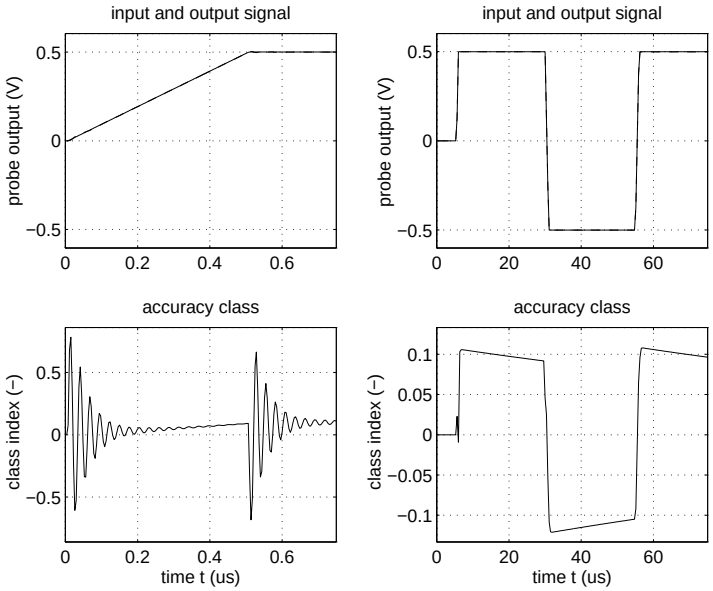

Fig. 11 : Time domain simulation, I_{max} = 500 A, Rd = 50 kOhm, di/dt=1kA/us

3 Prototype

The new principle has been implemented in a current probe prototype. The evaluation circuit as well as the coil and the Hall sensors are on the same PCB. The windings of the coil are formed through the upper and lower side copper strip and at each end they are connected by vias. The return wire is placed on an intermediate layer Fig. 3. The Hall sensors are placed on the top side of the multi layer board as well as the remaining surface mounted component devices (SMD's) required for the evaluation circuit. To shield the sensor from stray electric fields the PCB was placed in an aluminum box. Fig. 12 shows the prototype current sensor.

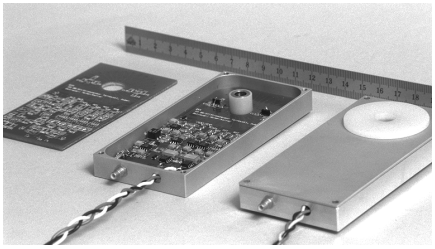

Fig. 12 : Probe prototype

This probe needs an accurate active low-pass. Since a low-pass TF is requested the design of the circuit with a high gain of 1000 can be accomplished.

4 Measurement

In Fig. 13 on the left side the low frequency performance is demonstrated. The output of the HOKA probe is compared against three well known current probes. On the left side the high frequency performance is demonstrated. The measured di/dt is about 2.5 kA/us. In both cases the relative error was computed with (14) choosing one of the standard current sensors as reference.

$$err(t) = \left(\frac{I_{\text{reference}}(t) - I_{\text{HOKA}}(t)}{200\,\text{A}} \right) 100\% \quad (14)$$

For the low frequency signal the ILA SMZ 200 and for the high frequency the LEM 25/10 coaxial shunt has been chosen as reference. The maximum error was +/- 5% in both cases referring to the sensors nominal current of 200 A. This means that the sensor belongs to the accuracy class 5.

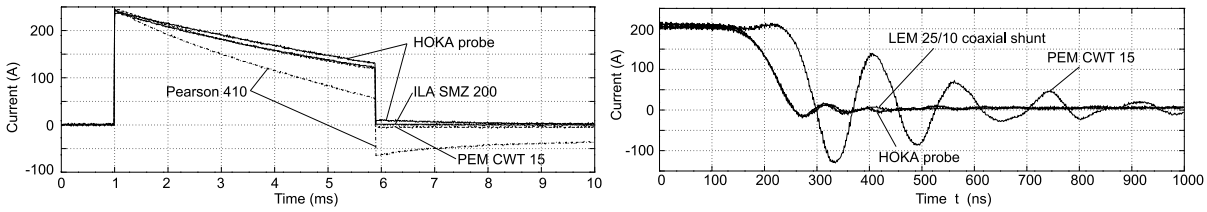

Fig. 13 : Current measurement comparison

5 Conclusion

An isolated current probe based on the new measurement principle HOKA is presented. Merging the output signal of a Hall sensor with a Rogowski coil, enlarges the bandwidth of each sensor. This new probe can measure DC currents as well as di/dt of several kA/us. A relationship between accuracy class, di/dt and undamped natural coil frequency is given. The evaluation circuit, which merges the output signals of the two sensors consists of an active low-pass. A current probe prototype based on this principle was built for a nominal current of 200 A. The probe demonstrated an accuracy class 5 behavior for DC signals and transients up to 2.5 kA/us. Further research will be performed in order to increase the probe's performance.

References

1. P. HOFER-NOSER and N. KARRER. *Monitoring of paralleled IGBT/diode modules*, IEEE Trans. on Power Electronics, May 1999, in press.
2. *Magnetic Sensors – Data Book*, Siemens, München 81541, Germany, pp. 66-68, July 1996.
3. K. HEUMANN. *Messung und oszillographische Aufzeichnung von hohen Wechsel- und schnell veränderlichen Impulsströmen*, Techn. Mitt. AEG-TELEFUNKEN, vol. 60, no. 7, pp 444-448, 1970.
4. A. RADUN. *An alternative low-cost current-sensing scheme for high-current power electronics circuits*, IEEE Trans. on Industrial Electronics, vol. 42, no. 1, pp.78-84, February 1995.
5. W.F. RAY. *Rogowski transducers for high bandwidth high current measurement, IEE Colloquium on Low Frequency Power Measurement and Analysis*, pp. 10/1-10/6, November 1994.
6. W.F. RAY. *Wide bandwidth Rogowski current transducer, part II: The integrator*, EPE Journal, vol. 3, no. 2, pp. 116-122, June 1993.
7. A.P. CHATTOCK. *On a magnetic potentiometer*, Philosophical Magazin and Journal of Science, vol. XXIV, 5th Series, pp. 94-96, Jul-Dec 1887.
8. W. ROGOWSKI and W. STEINHAUS. *Die Messung der magnetischen Spannung*, Archiv für Electrotechnik, vol. 1, no. 4, pp. 140-150, 1912.
9. N. KARRER and P. HOFER-NOSER. *A new current measuring principle for power electronic applications*, Proc. ISPSD 99, Toronto, 1999, in press.